A Super-Resolved View of the Alzheimer's Disease-Related Amyloidogenic Pathway in Hippocampal Neurons

Yang Yu[a], Yang Gao[a], Bengt Winblad[a,b], Lars O. Tjernberg[a] and Sophia Schedin-Weiss[a,*]

[a]*Division of Neurogeriatrics, Department of Neurobiology, Care Sciences and Society, Karolinska Institutet, Solna, Sweden*
[b]*Theme Inflammation and Aging, Karolinska University Hospital, Huddinge, Sweden*

Abstract.

Background: Processing of the amyloid-β protein precursor (AβPP) is neurophysiologically important due to the resulting fragments that regulate synapse biology, as well as potentially harmful due to generation of the 42 amino acid long amyloid β-peptide ($A\beta_{42}$), which is a key player in Alzheimer's disease.

Objective: Our aim was to clarify the subcellular locations of the fragments involved in the amyloidogenic pathway in primary neurons with a focus on $A\beta_{42}$ and its immediate substrate AβPP C-terminal fragment (APP-CTF). To overcome the difficulties of resolving these compartments due to their small size, we used super-resolution microscopy.

Methods: Mouse primary hippocampal neurons were immunolabelled and imaged by stimulated emission depletion (STED) microscopy, including three-dimensional three-channel imaging, and quantitative image analyses.

Results: The first (β-secretase) and second (γ-secretase) cleavages of AβPP were localized to functionally and distally distinct compartments. The β-secretase cleavage was observed in early endosomes in soma, where we were able to show that the liberated N- and C-terminal fragments were sorted into distinct vesicles budding from the early endosomes. Lack of colocalization of $A\beta_{42}$ and APP-CTF in soma suggested that γ-secretase cleavage occurs in neurites. Indeed, APP-CTF was, in line with $A\beta_{42}$ in our previous study, enriched in the presynapse but absent from the postsynapse. In contrast, full-length AβPP was not detected in either the pre- or the postsynaptic side of the synapse. Furthermore, we observed that endogenously produced and endocytosed $A\beta_{42}$ were localized in different compartments.

Conclusion: These findings provide critical super-resolved insight into amyloidogenic AβPP processing in primary neurons.

Keywords: $A\beta_{42}$, Alzheimer's disease, amyloid-β protein precursor, stimulated emission depletion microscopy, synapse

INTRODUCTION

Deciphering the molecular landscape of vesicular trafficking and synaptic dysfunction is crucial for understanding the complexity of neurons in physiology and disease. Until recently, light microscopic techniques have been hampered by a resolution limit of around 200 nm, which is insufficient for precise visualization of the subcellular compartments. The emerging super-resolution microscopy techniques enable examination of the architecture of synapses and fine structure of organelles at the low nanoscale level. These revolutionizing tools will be critical for understanding the biological systems in the brain and for mapping the pathological processes underlying neurodegenerative disorders, among which Alzheimer's disease (AD) is the most common one.

Amyloid-β peptide (Aβ) is a key player in AD and the main constituent of amyloid plaques [1]. This 40–43 residue long peptide is derived from the amyloid-β protein precursor (AβPP), a type 1

*Correspondence to: Sophia Schedin-Weiss, Karolinska Institutet, Department of NVS, Division of Neurogeriatrics, Solna, Sweden. Tel.: +46 73 0462626; E-mail: sophia.schedin.weiss@ki.se.

transmembrane protein suggested to be involved in synaptic function, neurite growth, vesicle transport, and cell-cell interactions (reviewed in [2]). The processing of AβPP occurs by either a non-amyloidogenic or an amyloidogenic pathway. In addition, AβPP can be cleaved in other, less thoroughly described pathways, such as meprin-β cleavage, the δ-pathway and the η-pathway (reviewed in [3]). As a result, various fragments of AβPP can be formed. In the amyloidogenic pathway, AβPP is first cleaved by β-secretase (BACE1) to generate soluble AβPPβ (sAβPPβ) and a 99 amino acids long membrane bound C-terminal fragment (CTF) denoted C99. The latter is subsequently processed by a transmembrane enzyme complex named γ-secretase, releasing AβPP intracellular domain (AICD) into the cytosol and monomeric Aβ (mainly $A\beta_{40}$ and $A\beta_{42}$) into the vesicular lumen [4]. Although $A\beta_{42}$ can be a causative agent in AD [5], the molecular details behind its neurotoxicity are largely unknown. Studies during the past two decades have shown that intracellular $A\beta_{42}$ is neurotoxic [6, 7] and plays an important role in the AD process [8, 9]. Importantly, oligomers formed by Aβ are especially toxic to neurons and can bind to cell surface receptors at neuronal synapses [10, 11], affect the synaptic structure, spread from neuron to neuron and are associated with cognitive decline in AD [12, 13]. Furthermore, plaques formed by fibrillar Aβ can induce synaptic dysfunction, inflammatory response (microglia and astrocytic activation) and neuronal injury, eventually leading to neurodegeneration [14]. Apart from the role in AD pathology, Aβ may play a significant role in normal synaptic function [15, 16]. Thus, it is important to study the synthesis, subcellular location, transport and function of Aβ both from a physiological and pathological perspective.

Several studies on the processing of AβPP into Aβ and the subcellular compartments involved in this process have been reported. However, most of these studies are not fully conclusive since they have been performed in cell lines and not in neurons, and the studies trying to pinpoint the subcellular location of Aβ and its precursors have been limited by the insufficient resolution obtained by standard confocal microscopes. Still, a crude picture of the processing has emerged. For instance, several studies suggest that the generation and trafficking of Aβ is related to the endosomal/lysosomal system, including early endosomes, recycling endosomes, late endosomes (including multivesicular bodies (MVBs)), and lysosomes [17–20]. Intraluminal vesicles (ILVs)

stored in MVBs, and subsequently released as exosomes [21], have been suggested to be one way by which Aβ is secreted [22]. Moreover, autophagy has been suggested to be related to Aβ production and release by influencing the intracellular Aβ generation, trafficking and secretion [7, 23]. Some studies suggest that neuronal Aβ is produced at the synapse, and that AβPP can be transported along axons [24, 25].

Electron microscopy (EM) has been used to visualize Aβ and related proteins in human and mouse brain. For instance, EM was used to elucidate the subcellular localization of $A\beta_{42}$ in the endosomal-lysosomal pathway [26], and to show intraneuronal accumulation of $A\beta_{42}$ in MVBs in mouse brain. Interestingly, the level of $A\beta_{42}$ at the presynapse was found to increase with aging [27]. Although EM is advantageous by providing a high resolution, it is also accompanied by limitations in labeling density as wells as the number of different molecules that can be imaged simultaneously, and it is difficult to use EM for three-dimensional (3D) studies and live cell imaging of neurons.

Using the super-resolution microscopy technique stimulated emission depletion (STED) microscopy, we recently resolved the pre- versus postsynaptic localization of γ-secretase and $A\beta_{42}$ in primary hippocampal neurons [28, 29]. Here, we pushed the application of STED microscopy further and included 3D 3-channel STED imaging and vesicular markers to visualize the components of the amyloidogenic machinery in soma, neurites and synapses of mouse primary hippocampal neurons. With this approach, we were able to localize the sorting of N- and C-terminal AβPP fragments to early endosomes, demonstrate that APP-CTF is strictly localized to the presynaptic side of the synapse and characterize different intraneuronal pools of $A\beta_{42}$. These findings are critical for understanding the role of AβPP processing in neuronal functions and in AD pathogenesis.

MATERIALS AND METHODS

Reagents

The following reagents were used: Hanks' Balanced Salt Solution (HBSS, Gibco); Dulbecco's phosphate-buffered saline (DPBS, Gibco); Neurobasal medium (Gibco); B27 (Thermo Fisher); L-glutamine (Gibco); Poly-D-lysine (P7405; Sigma); Formaldehyde (Sigma); CHAPSO (Merck Millipore); 10% normal goat serum (NGS, Invit-

rogen); Tween (Gibco); Glutaraldehyde (Sigma); ProLong gold antifade reagent (Life Technologies); HiLyte™ Fluor 647 - $A\beta42$ (AnaSpec).

Antibodies

The Y188 antibody targeting the C-terminus of $A\beta PP$ (APP-CT) was used to visualize full-length $A\beta PP$ and CTFs. In order to study the localization of $A\beta_{42}$ in neurons, it is essential to find an antibody that is specific for $A\beta_{42}$, and does not react with $A\beta_{40}$, $A\beta_{43}$, $A\beta PP$, APP-CTFs or APP-NTFs. In this study, we used a rabbit antibody, which is specific for the C-terminal neo-epitope of $A\beta_{42}$. This antibody has previously been thoroughly characterized and shown not to have cross-reactivity with $A\beta_{40}$, APP-CTF or full-length $A\beta PP$ [29, 30]. To further validate these antibodies, immunohistochemistry was performed with $A\beta PP$ knock-out (K/O) mice brain compared with wild type (WT) mice brain sections (Supplementary Figure 1). Thus, the specificity was confirmed for the APP-CT antibody (Y188, Supplementary Figure 1A) and the $A\beta_{42}$ antibody (Supplementary Figure 1B) in $A\beta PP$ K/O mice. The N-terminus of $A\beta PP$ was detected using the antibody 22C11 (which cross-reacts with the N-terminus of APLP2). All primary antibodies used in this study are shown in Table 1. Secondary antibodies are shown in Table 2.

Mice

C57BL/6 mice were used for culturing of WT hippocampal neurons. $A\beta PP$ K/O adult mice (Jackson Labs, Maine, USA, JAX 004133) [31] were used to make brain sections.

Culturing of primary hippocampal neurons

Mouse embryos (16–17 days) were taken from pregnant mice and stored in cold HBSS buffer. Cortex and hippocampus were dissected as described previously [29]. Hippocampal neurons were seeded at the center of 35 mm glass bottom culture dishes (P35-G-1.5-10-C; MatTek), pre-coated with poly-D-lysine, and a support layer of cortical neurons was seeded at the edges of the plate, essentially as described previously [28, 29, 32]. Neurobasal medium with 2% B27 and 1% L-glutamine were used for culturing. After 21 days, when the hippocampal neurons are mature and have developed an extensive network of neurites and synapses, they were fixed and used for other experi-

Table 1
Primary antibodies used in this study

Antibody	Species	Target	Cat No.	Dilution	Source
Y188	R	APP-CT	Ab32136	1:50	Abcam
$A\beta42$	R	C-terminus of $A\beta42$	NA*	1:200/400	In house
22C11	M	APP-NT	3043557	1:250	MERCK
Clathrin heavy chain	M	Clathrin	Ab2731	1:100	Abcam
EEA1	GP	Early endosomes	237105	1:500	Synaptic Systems
Rab7	M	Lysosomes/LEs	Ab50533	1:500	Abcam
Rab9	M	LEs/lysosomes	Ab2810	1:200	Abcam
Rab3	M	Synaptic vesicles	107011	1:50	Synaptic Systems
Rab26	M	Recycling endosomes	269011	1:50	Synaptic Systems
LC3A	M	Autophagosomes	3233-100	1:200	BioVision
Flotillin1 (FLOT1)	M	Exosomes	610820	1:100	BD Biosciences
VAMP2	R	Synaptic vesicles	104202	1:500	Synaptic Systems
PSD95	M	Postsynaptic density	Ab2723	1:200	Abcam
Synaptophysin (syn)	M	Synaptic vesicles	08311616	1:500	Enzo Life Sciences

*Not applicable; Les, late endosomes; GP, guinea pig; R, rabbit; M, mouse; Cat No., catalogue number.

Table 2
Secondary antibodies and probes used in this study

Fluorophore	Target	Cat No.	Dilution	Source
Alexa Fluor 594	anti-mouse	2110496	1:200	Invitrogen
Abberior STAR 635P	anti-rabbit	2-0012-007-2	1:200	Abberior
Alexa Fluor 594	anti-guinea pig	2079357	1:200	Invitrogen
Fab TRITC	anti-mouse	A24523	1:200	Invitrogen
Fab Alexa Fluor 647	anti-rabbit	1829925	1:200	Invitrogen
Alexa Fluor 488	anti-mouse	861163	1:200	Invitrogen
Alexa Fluor 488 Phalloidin	actin	2129460	1:100	Invitrogen

ments. Each batch of neuronal cultures included three embryo brains without distinction between male and female mice and, thus, could be mixed cultures.

Sample preparation for STED and confocal microscopy

Hippocampal neurons cultured for 21 days were fixed for 10 min with 4% formaldehyde in neurobasal medium, pre-heated to 37°C, followed by washing with DPBS three times. Fixed samples were permeabilized with 0.4% CHAPSO for 10 min, blocked with 10% normal goat serum (NGS) for 15 min and incubated with primary antibodies overnight at 4°C. Samples were rinsed with DPBS three times and then incubated with secondary antibodies in 3% NGS for 2 h at room temperature. After incubation with secondary antibodies, the samples were washed with PBS containing 0.1% Tween (PBST) three times and with DPBS three times. The labelled samples were postfixed with a solution containing 0.1% glutaraldehyde and 3% formaldehyde for 10 min. After washing by DPBS and water, the samples were mounted with ProLong gold antifade reagent and stored at 4°C until imaging. Individual experiments were performed three times for each type of staining.

Labeling with live cell endosomal and lysosomal markers

CellLight Early Endosome-green fluorescent protein (GFP) and CellLight Late Endosome-red fluorescent protein (RFP) BacMam 2.0 (Invitrogen) were added to the medium of the primary hippocampal neurons to a final concentration of 5 and 7.5 particles per cell, respectively, based on our optimized protocol. The cells were incubated (37°C, 5% CO_2) for at least 24 hours to obtain sufficiently high transduction efficiency. Lysosomes were labeled by treating cells with 100 nM SiR-lysosome (Spirochrome AG) at 37°C, 5% CO_2 for 6 h, according to the manufacturer's protocol.

Sample preparation of brain tissue for immunohistochemistry

To validate the specificity of the $A\beta_{42}$ and APP-CTF antibodies, brain sections from $A\beta$PP K/O mice and WT mice were used for immunolabeling. $A\beta$PP K/O and WT mouse brains were from Gunnar Gouras' Lab, Lund University. Brains were stored in 30% sucrose solution during transfer. The brains were frozen with optical cutting temperature (OCT) onto the metal grids fitting the cryostat, cut into 10 μm sections at –20°C and transferred to a room temperature imaging slide. These slides were used directly for immunohistochemistry or stored at –20°C (short-term storage) until used.

Samples were permeabilized with 0.4% CHAPSO and blocked with 10% NGS followed by incubation with $A\beta_{42}$ antibody (dilution 1:1000) or APP-CT antibody (dilution 1:1000) overnight at 4°C. On the second day, the samples were incubated with secondary antibody (Abberior STAR 635P) and imaged by confocal microscopy.

STED imaging

STED imaging was performed with a Leica TCS SP8 STED 3X (Leica Microsystems) equipped with a HCPLAPO100x/1.40 Oil STED WHITE objective. For 2-color STED imaging, the fluorophores Alexa Fluor 594 and Abberior STAR 635P were excited by a pulsed white light laser with lines at 598 nm and 653 nm, respectively. The pulsed STED laser at 775 nm was used for both imaging channels. A confocal channel excited at 488 nm was also used to outline the cellular structure by actin staining with Phalloidin labelled with Alexa Fluor 488. The channels were recorded sequentially with a pixel size of 25 nm at line scan speeds of 200–400 Hz. Three-color STED microscopy was applied with fluorophores Alexa Fluor 594, Abberior STAR 635P and TRITC, excited by pulsed white light lasers lines at 598 nm, 653 nm and 540 nm, respectively, and depleted with 775 nm laser light. STED imaging with both 2D vortex and 3D phase-ring pattern were applied to improve the resolution in the imaging plane and along the optical axis.

Data analysis

Images taken by confocal or STED microscopy were analyzed by ImageJ. All pictures except colocalization analysis shown are raw data, except for stretching the contrast. For colocalization analysis, images were subjected to thresholding using the Otsu or Moments function. 3D videos were made by Leica STED software or Imaris. 3D image analysis was made by Huygens professional "small particles geometry" to analyze the vesicles. The filter "remove all vesicles that are non-colocalized" was used. All graphs were made by GraphPad.

RESULTS

We previously showed that STED microscopy, in contrast to confocal microscopy, can be used to resolve different types of Aβ$_{42}$-containing vesicles such as small Aβ$_{42}$-containing vesicles in the presynapse and larger vesicles with Aβ$_{42}$ only at the rim in other regions [29]. In this study, we have analyzed which types of vesicles contain Aβ$_{42}$ by including subcellular markers. We have also continued our quest to reveal the subcellular details of amyloidogenic AβPP processing by using state-of-the-art STED microscopy and pushed the limits to include 3D 3-channel STED microscopy. Thus we have determined the intraneuronal localization of also the substrate, AβPP. We used a validated commercial antibody specific for the C-terminus of AβPP (APP-CT) that binds to full-length-AβPP and APP-CTF. The Aβ$_{42}$ antibody used is specific for the C-terminal neo-epitope of Aβ$_{42}$, has been thoroughly characterized and does not cross-react with other forms of Aβ, AβPP, or APP-CTF [29, 30]. The specificities of these antibodies were further confirmed here by immunohistochemistry of AβPP K/O mice (Supplementary Figure 1). In some experiments we also included an antibody targeting the N-terminus of AβPP (APP-NT). The antibodies used to label various organelles are shown in Table 1.

By analyzing a large number of STED images of mouse primary hippocampal neurons stained with the APP-CT or Aβ$_{42}$ antibodies and several subcellular markers, we have elucidated the subcellular localizations of AβPP, CTFs, and Aβ$_{42}$ in soma, neurites, and synapses of hippocampal neurons. Actin staining was used to visualize the morphology of the neurons, enabling selection of synapses where the pre- and postsynaptic sides are located side-by-side with the spine extended in the xy plane (to avoid the risk of false positive overlap along the z-axis). Healthy neurons were selected from the actin staining in confocal mode (Supplementary Figure 2). For optimal resolution, STED imaging was performed by cropping the field of view.

Endocytosis of AβPP occurs by a clathrin-mediated pathway

First, we evaluated the localization of APP-CT in the clathrin-mediated endocytic pathway in the soma and found considerable colocalization of APP-CT with clathrin (Fig. 1A-D). A representative structure in which APP-CT was partially surrounded by clathrin was subjected to plot intensity analysis, which showed that the diameter of this structure was around 250 nm (Fig. 1E, F). The APP-CT-containing structures enclosed by a semi-circular clathrin coat with a diameter of around 250 nm probably represent clathrin-coated pits (CCPs), in line with previous studies using STORM and STED microscopy to visualize such structures [33, 34]. The smaller vesicles observed in Fig. 1A presumably represent clathrin-coated vesicles (CCVs), in line with previous findings reporting diameters of CCVs in soma to be around 90 nm [35]. Note that the labeling by primary and secondary antibodies results in apparently larger structures due to the size of the immuno-complex. Even larger clathrin-coated structures, up to 600 nm, some of which potentially correspond to clathrin patches on a multivesicular body [35] were also found. In soma, 30% of APP-CT staining colocalized with clathrin and, interestingly, as much as 85% of the clathrin colocalized with APP-CT (Fig. 1G). These findings support the notion that the clathrin-mediated pathway is crucial for endocytosis of AβPP.

Next, the presence of APP-CT in clathrin-coated structures was evaluated in neurites (Fig. 1H-K). The colocalization pattern of APP-CT along neurites appeared to follow mainly axonal structures with enrichment observed close to or at presynapses. In contrast to soma, the smaller structures dominated in neurites (Fig. 1L, M), in line with earlier studies reporting a diameter of 40 nm for CCVs in axon terminals [35], suggesting that the ratio of CCPs to CCVs was lower in neurites than in soma.

AβPP fragments are sorted in early endosomes

To investigate the presence and localization of AβPP and AβPP fragments in early endosomes, we imaged the APP-NT, APP-CT, and EEA1 markers by 3-color STED microscopy to obtain super-resolution in all three channels (Fig. 2A). The EEA1 staining was present at the rim of the early endosome while APP-CT appeared in concentrated regions (referred to as clusters below) within or at the edge of the early endosomes. Due to the high resolution, it is truly possible to discriminate between clusters that contain only C-, only N-terminal fragments or both (zoomed-in pictures in Fig. 2B, C). Analysis of several zoomed-in images showed that the early endosomes contain different combinations of AβPP fragments (Fig. 2B, C and Supplementary Figure 3). 70% were positive for both APP-CT and APP-NT, suggesting that they contain full-length AβPP, while
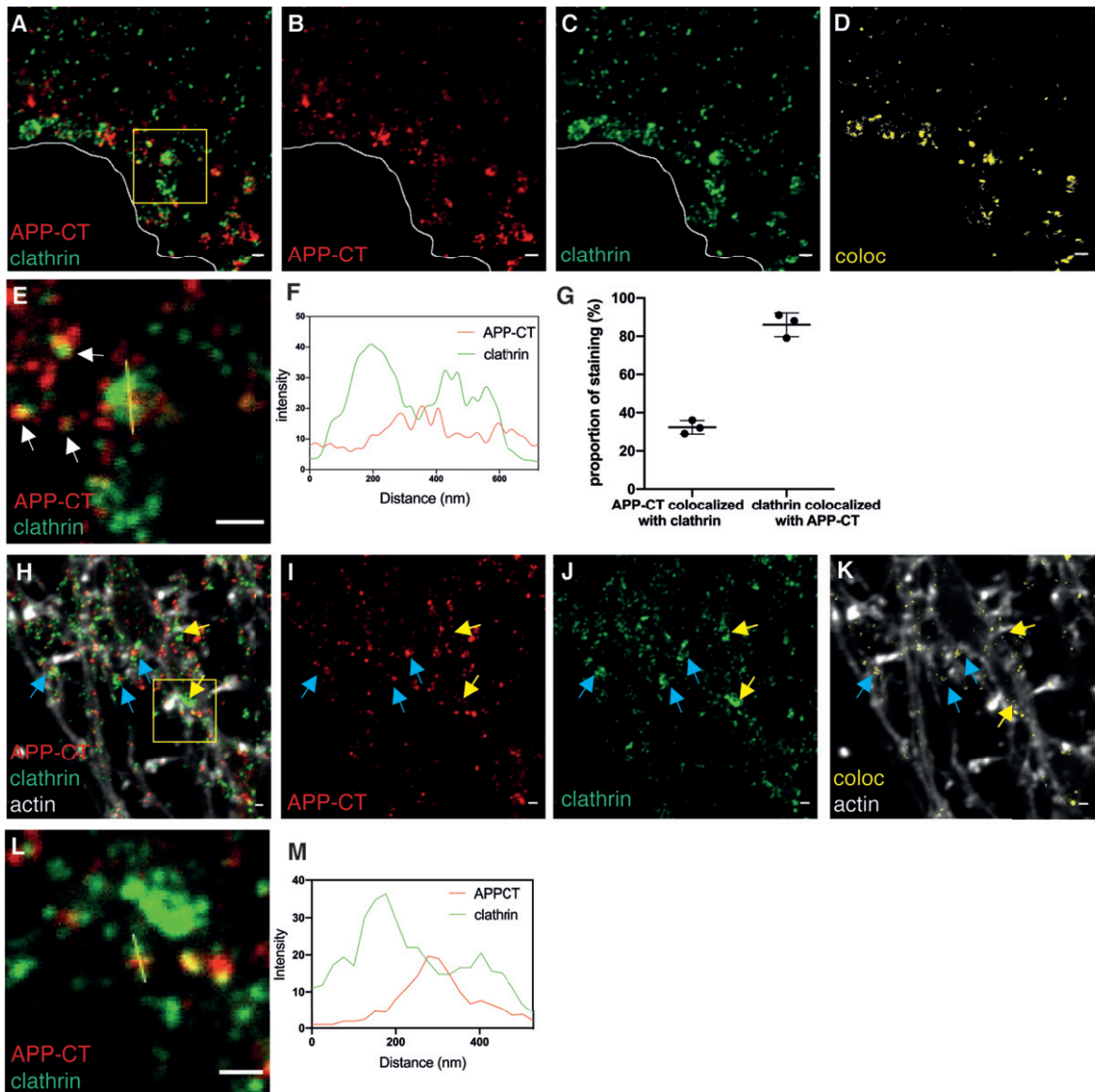
Fig. 1. STED images of APP-CT in clathrin-coated pits and clathrin-coated vesicles in soma and neurites. Immunolabeling and 2-channel STED imaging was used to visualize the subcellular localization of APP-CT and clathrin in hippocampal neurons. A third, confocal, channel was used to image the actin cytoskeleton (phalloidin staining). Scale bar for all pictures: 500 nm. A-D) APP-CT (red) and clathrin (green) in soma. The border of the cell is marked in white. Images show, from left to right, A) both channels, B) APP-CT, and C) clathrin, respectively. D) The areas with colocalization of APP-CT and clathrin in (A) is shown in yellow. E) Zoomed-in image of the region marked with a yellow square in (A). Small vesicles with APP-CT staining partially colocalized with clathrin are marked with white arrows, while APP-CT enclosed by a coat of clathrin in a half-spherical shape is marked with a yellow line. F) Plot intensity analysis of the signal along the yellow line in (E). G) Percentage of total APP-CT staining in soma that colocalized with clathrin and of total clathrin staining in soma that colocalized with APP-CT. Data were quantified from 3 samples, cultured from different batches of mice embryos. All error bars represent mean ± sd. Analysis was done by "particle analyze" in ImageJ. Threshould "Moments" was applied for the Aβ42 channel. Threshould "Triangle" was applied for the clathrin channel. H-J) APP-CT (red) and clathrin (green) in neurites, combined with actin staining in white to show the outline of the neurites (the latter imaged by confocal microscopy). Images show, from left to right, H) all channels, I) APP-CT, and J) clathrin. Some spots of colocalization for APP-CT and clathrin are marked with blue arrows, while structures containing clathrin but not APP-CT are marked with yellow arrows. K) Colocalization of APP-CT and clathrin are shown in yellow. L) Zoomed-in image of the structure marked by the yellow square in (H). The brightness was increased by ImageJ in order to see the weak signal. M) Plot intensity analysis of the signal along the yellow line in (L).
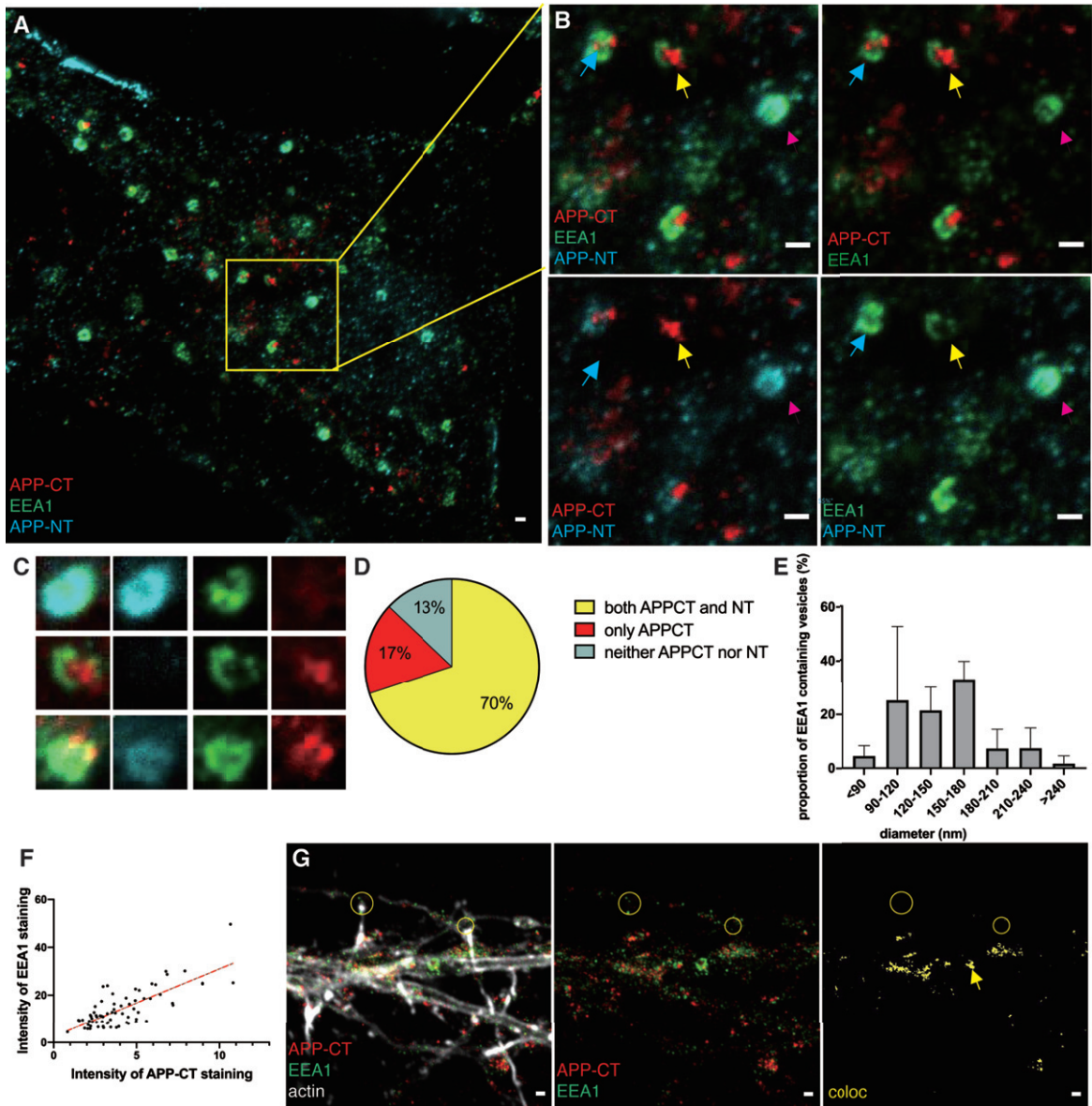
Fig. 2. STED images of APP fragments in early endosomes. Immunolabeling and 2- or 3-channel STED microscopy was used to visualize the subcellular localization of APP-CT and/or APP-NT and the early endosome marker EEA1 in hippocampal neurons. 2-channel STED imaging was combined with a third confocal channel to image the actin cytoskeleton (phalloidin staining). Scale bar for all pictures: 500 nm. A) 3-channel STED images of APP-CT (red), APP-NT (cyan) and EEA1 (green) in soma. B) Zoomed-in field and separate channels. Yellow arrows point at vesicles containing APP-CT but not APP-NT. Magenta arrows point at vesicles containing APP-NT but not APP-CT. Blue arrows point at vesicles containing both APP-CT and APP-NT. C) 3-channel STED images of zoomed-in early endosomes visualizing EEA1 (green), APP-CT (red) and APP-NT (cyan) showed in merged and separate channels. D) Quantification of APP-CT and/or APP-NT in EEA1-positive early endosomes ($n = 70$). E) Quantification of the size (diameter) of EEA1-positive vesicles. Data were quantified from 5 different batches of hippocampal neurons. All error bars represent mean ± sd. F) Quantification of the intensity of EEA1 and APP-CT staining in soma ($n = 70$). G) 2-channel STED images of APP-CT (red) and EEA1 (green) in neurites overlayed with actin shown in a confocal channel. Images show, from left to right, all channels, APP-CT and EEA1, colocalization of APP-CT and EEA1. Lack of colocalization in two synaptic regions are marked by yellow circles. The yellow arrow points out the large EEA1-containing vesicle.

17% contained only APP-CTF and 13% contained neither full-length AβPP nor APP-CTF (Fig. 2D). Since EEA1 is a peripheral membrane protein of early endosomes, we measured the inner part of EEA1 ring-like staining to calculate the size. Thus, the diameter of the early endosome ranged from 90 to 240 nm

(Fig. 2E). The density of the APP-CT staining in early endosomes varied. Using image analysis, we found a positive correlation between the intensity of EEA1 and APP-CT staining, demonstrating that the early endosomes that bind to more EEA1 also have more APP-CTF (Fig. 2F). More examples of zoomed-in images of early endosomes are shown in Supplementary Figure 3. Various morphologies of APP-CTF staining could be observed. A few of these contained no detectable APP-CTF (Supplementary Figure 3A) while most of them contained one or several APP-CTF clusters (Supplementary Figure 3B, C). For some of the endosomes, these clusters were located inside or at the edge of the endosomes, while others had clusters very close to, but outside, the endosomes. Similar findings were observed for APP-NTF. These findings indicate that sorting of AβPP fragments occur in early endosomes.

In neurites, most early endosomes were smaller than in the soma (Fig. 2G), and the larger ring-like structures were rarely detected. Colocalization of APP-CTF and the early endosomal marker EEA1 was observed in soma and in neurites, but not in the presynapse.

Due to the interesting morphology of the early endosomes observed with STED imaging, we next used 3D-three-channel STED microscopy to further improve the resolution along the z-axis and visualize AβPP and AβPP fragments in three dimensions (the trade-off being a slightly lower resolution in the xy plane). A resulting 3D movie shows the staining of APP-CT, APP-NT, and early endosomes in soma (Supplementary Video 1). One striking observation was that the majority of APP-CT and APP-NT did not colocalize, suggesting that early endosomes contain a larger proportion of N- and C-terminal fragments than full-length AβPP. Images of early endosomes and AβPP fragments containing 3D information are shown in Fig. 3. For 3D data, all colocalization analyses were voxel-based morphometry, limited to two fluorescence channels at the same time. As observed with 2D-STED microscopy, a large proportion of APP-CT were present in early endosomes in soma (Supplementary Figure 4A). A filter that automatically removes all vesicles containing only EEA1 or APP-CT, leaving only early endosomes that contain APP-CT, was subsequently applied (Fig. 3A). The zoomed-in area is shown from three different angles (Fig. 3B and Supplementary Figure 4B-D). Using the same approach, we showed colocalization of vesicles containing APP-NT and APP-CT (Fig. 3C, D and

Supplementary Figure 4E-H) or APP-NT and EEA1 (Fig. 3E, F and Supplementary Figure 4I-L). These images show clusters of APP-CTF concentrated at or close to one portion of the surface, while the N-terminal staining was concentrated at another portion of the surface. These structures seemed to be budding from the early endosomes, suggesting that the early endosomes pack and sort the different types of AβPP fragments into different types of transport vesicles that are trafficked in different directions (see our proposed model in Fig. 3G).

By using Rab9 antibody as a marker for late endosomes we found little overlap with APP-CT staining in soma (Supplementary Figure 5A) and no colocalization in neurites (Supplementary Figure 5B). Thus, we suggest that the majority of APP/APP-CTFs in the soma are present in clathrin-coated vesicles or early endosomes.

AβPP C-terminal fragments are strictly localized to the presynaptic side of synapses

To investigate the localization of APP-CT in synapses, we labelled samples with APP-CT, APP-NT, and synaptic markers and imaged them by STED microscopy. Actin was visualized in a confocal channel. Images in which the pre- and postsynaptic sides were separated in the x-y plane were selected. The separation of the pre- and postsynaptic sides could be clearly observed. No colocalization was observed between APP-CT and PSD95, demonstrating that neither full-length AβPP nor its C-terminal fragments are present in the postsynapse (Fig. 4A). In contrast, extensive overlap was observed between APP-CT and synaptophysin (Fig. 4B). The APP-CT was also present in pre-presynapses, i.e., structures that contain presynaptic proteins but have not connected to dendrites (Fig. 4B). The APP-NT antibody was further used to visualize AβPP and its N-terminal fragments, combined with the presynaptic marker VAMP2, which revealed that neither full-length AβPP nor APP-NTF are present at the presynapse (Fig. 4C). Analyzing 30 fully developed synapses with the dendritic spines separated from presynaptic counterpart in the x/y plane (i.e., no overlap along the z-axis), we further confirmed our conclusion that APP-CTF is present at the presynapse while neither APP-CTF nor full-length AβPP are present in the postsynapse (Fig. 4D).
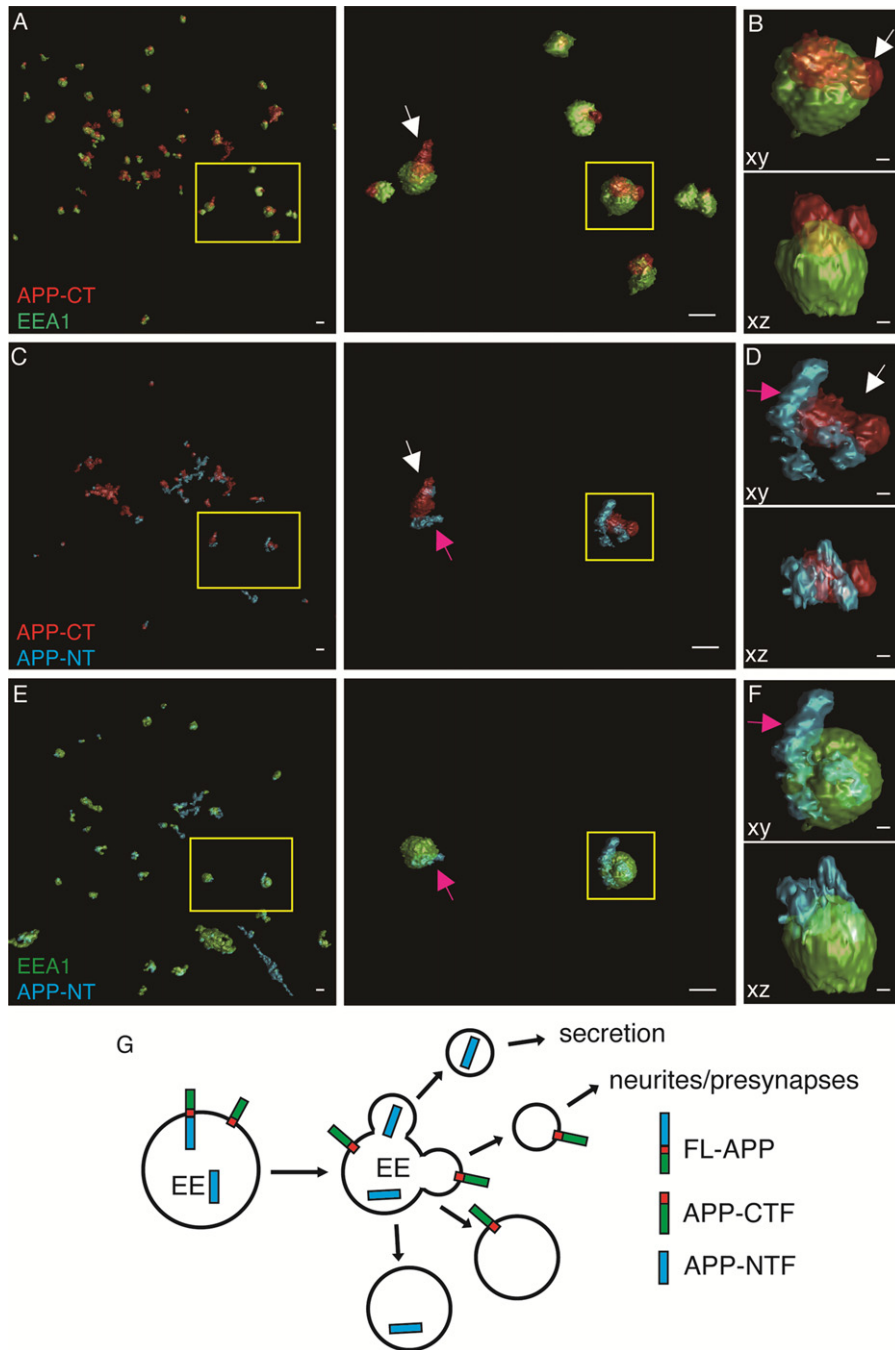
Fig. 3. 3D STED images of APP fragments in early endosomes in soma. Immunolabeling and 3D 3-channel STED microscopy was used to visualize AβPP and AβPP fragments in early endosomes in hippocampal neurons. Scale bars for A, C and E: 500 nm; scale bars for B, D and F: 100 nm. A, B) APP-CT and EEA1. C, D) APP-CT and APP-NT. E, F) APP-NT and EEA1. Using Huygens analysis software, a filter that can remove all non-overlapping vesicles was applied to show only the early endosomes that contain AβPP or AβPP fragments in A, C, and, E. Zoomed-in images of the regions marked by a yellow square in the left panel of A, C, and, E are shown in the middle panel and the selected vesicles marked by a yellow square in the middle panel are shown from two directions (xy, xz) in the right panel (B, D, and F). APP-CT budding from the early endosomes are marked by white arrows. APP-NT in the same early endosomes are marked by magenta arrows. All analyses were based on 3D data, which means that voxel-based practical colocalization analysis was applied. G) Schematic picture showing the sorting of AβPP fragments in early endosome.
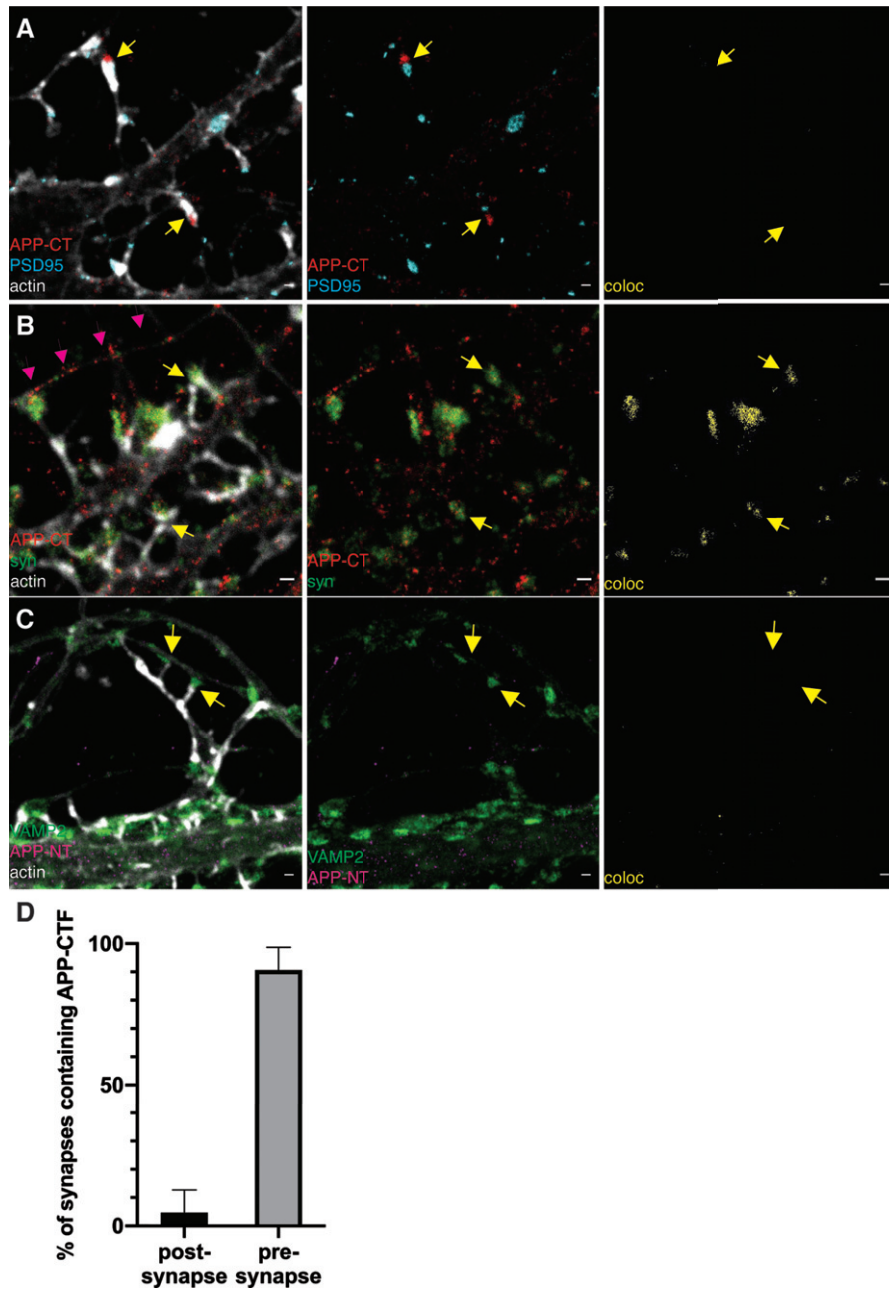
Fig. 4. STED images of APP-CTF and synaptic markers in neurites. Immunolabeling and 2-channel STED imaging was used to visualize APP-CTF and synaptic markers in neurites of hippocampal neurons. A third, confocal, channel was used to image the actin cytoskeleton (phalloidin staining). Scale bar for all pictures: 500 nm. A) APP-CT (red), PSD95 (cyan) and actin in a confocal channel (white). Synapses showing PSD95 at the postsynaptic spines and APP-CT at the presynaptic side are marked with yellow arrows. Images show, from left to right, all channels, APP-CT and PSD95 and colocalization of APP-CT and PSD95, respectively. The absence of yellow color indicates no colocalization. B) APP-CTF (red), synaptophysin (syn; green) and actin in a confocal channel (white). Synapses showing synaptophysin and APP-CT at the presynaptic side close to postsynaptic spines are shown by yellow arrows. Magenta arrows mark the staining of APP-CT in the "free" axon. Images show, from left to right, all channels, APP-CT and synaptophysin, colocalization of APP-CT and synaptophysin. C) APP-NT (magenta), VAMP2 (green) and actin in a confocal channel (white). The presynaptic side of two synapses is marked by yellow arrows. Images show, from left to right, all channels, APP-NT and VAMP2 and colocalization of APP-NT and VAMP2. D) Quantification of APP-CT in pre- or post-synaptic side. Data were quantified from 3 different batches of hippocampal neurons, 20 synapses for each. All error bars represent mean ± sd.

Characterization of Aβ_{42}-containing vesicles in soma

In our previous study using STED microscopy, we were able to resolve different types of Aβ_{42}-containing vesicles in mouse primary hippocampal neurons. The vesicles in the presynapse were small and partially co-localized with synaptic vesicles, while larger vesicles in other neuronal regions contained Aβ_{42} mostly on the rim [29]. Here, we characterized the Aβ_{42}-containing vesicles by combining immunostaining with vesicular marker immunostaining. First, we analyzed the colocalization with endosomal, lysosomal and autophagosomal markers in soma. In contrast to APP-CT, three-color STED imaging confirmed colocalization of Aβ_{42} with late endosomes but not with early endosomes (Fig. 5A). While some early endosomes that co-stained with Rab9 were also observed, the latter did not contain Aβ_{42} (zoomed inserts in Fig. 5A).

Lysosomal (Fig. 5B), autophagosomal (Fig. 5C), and/or recycling endosomal markers (Fig. 5D), all showed granular staining at the rim of Aβ_{42} vesicles. Small Aβ_{42} vesicles partially overlapped with flotillin-1 (Fig. 5E). Several individual flotillin-1 containing vesicles were found to be in close proximity to Aβ_{42}, suggesting that they may in fact be part of multivesicular bodies (Fig. 5E). Aβ_{42} was also observed in CCVs (Fig. 5F).

Image analysis showed that the majority of Aβ_{42}-containing vesicles are late endosomes or lysosomes, and around 20% of Aβ_{42}-containing vesicles are autophagosomes (Fig. 5H). The fact that the sum of the colocalization percent with Rab9, Rab7, and LC3 exceed 100% suggests that Aβ_{42} is present in organelles containing more than one type of subcellular marker, consistent with how vesicles mature through the endo-lysosomal system. The size of vesicles containing Aβ_{42} at the rim in the soma ranged with diameters from 100 to 900 nm, with one peak at 200 to 400 nm, and another peak at 600–700 nm (Fig. 5I).

Live cell markers confirm Aβ_{42} colocalization with late endosomes and lysosomes in soma

Since the immunolabeling density of EEA1, Rab9, and Rab7 was rather low, we confirmed our findings of Aβ_{42} localization in soma using live cell labelling of early and late endosomes and lysosomes. To label lysosomes, we used a Silicone Rhodamine-labelled fluorogenic probe specific for the lysosomal protein cathepsin D. Early endosomes were labelled via transduction with Rab5a-RFP and late endosomes/lysosomes via transduction with Rab7a-GFP. These experiments resulted in higher labelling density compared to the immunolabelling. However, these fluorophores do not meet the requirement of high photostability and brightness in STED microscopy, and thus, we used confocal microscopy with an Airyscan detector (providing two-fold improved resolution compared to confocal microscopy) after fixation of the live-labelled cells. Due to the relatively large size of these vesicles, the information obtained using the Airyscan system could be used to determine which of these organelles contain Aβ_{42} (Fig. 6), whereas STED was required to determine where in these vesicles Aβ_{42} is located. In soma, a large amount of Aβ_{42} was found in late endosomes/lysosomes (Fig. 6A), while no Aβ_{42} was observed in the early endosomes (Fig. 6B). Thus, these results confirm results from immunolabelling with organelle markers and demonstrate that Aβ_{42} in the soma is present in late endosomes and lysosomes but absent from early endosomes.

Aβ_{42} is present in different organelles in the synapse as compared to the soma

To further characterize the subcellular localization of Aβ_{42}-containing vesicles in hippocampal neurons, we used several subcellular markers for the endocytic-lysosomal-autophagosomal pathway to investigate the localization of Aβ_{42} in neurites and synapses.

In neurites, Aβ_{42} partially colocalized with clathrin. The extent of colocalization of Aβ_{42} and clathrin in the presynapse was highly variable ranging from 1% (Fig. 7A) to 17% (Supplementary Figure 5C), possibly reflecting differences in synaptic activity.

Colocalization of Aβ_{42} with EEA1 could be observed in neurites, except for the synapses (Fig. 7B). Interestingly, the colocalization was also present in "free" axonal boutons, which are not connected to dendritic spines (Fig. 7C). Aβ_{42} and Rab9 showed little colocalization in neurites (Fig. 7D). The vesicles in which Aβ_{42} colocalized with Rab9 had larger diameter (around 200–300 nm) than other non-overlapping Aβ_{42}-containing vesicles. Aβ_{42} showed similar colocalization with Rab7 as with Rab9. The Aβ_{42} vesicles that overlapped with Rab7 (Fig. 7E)
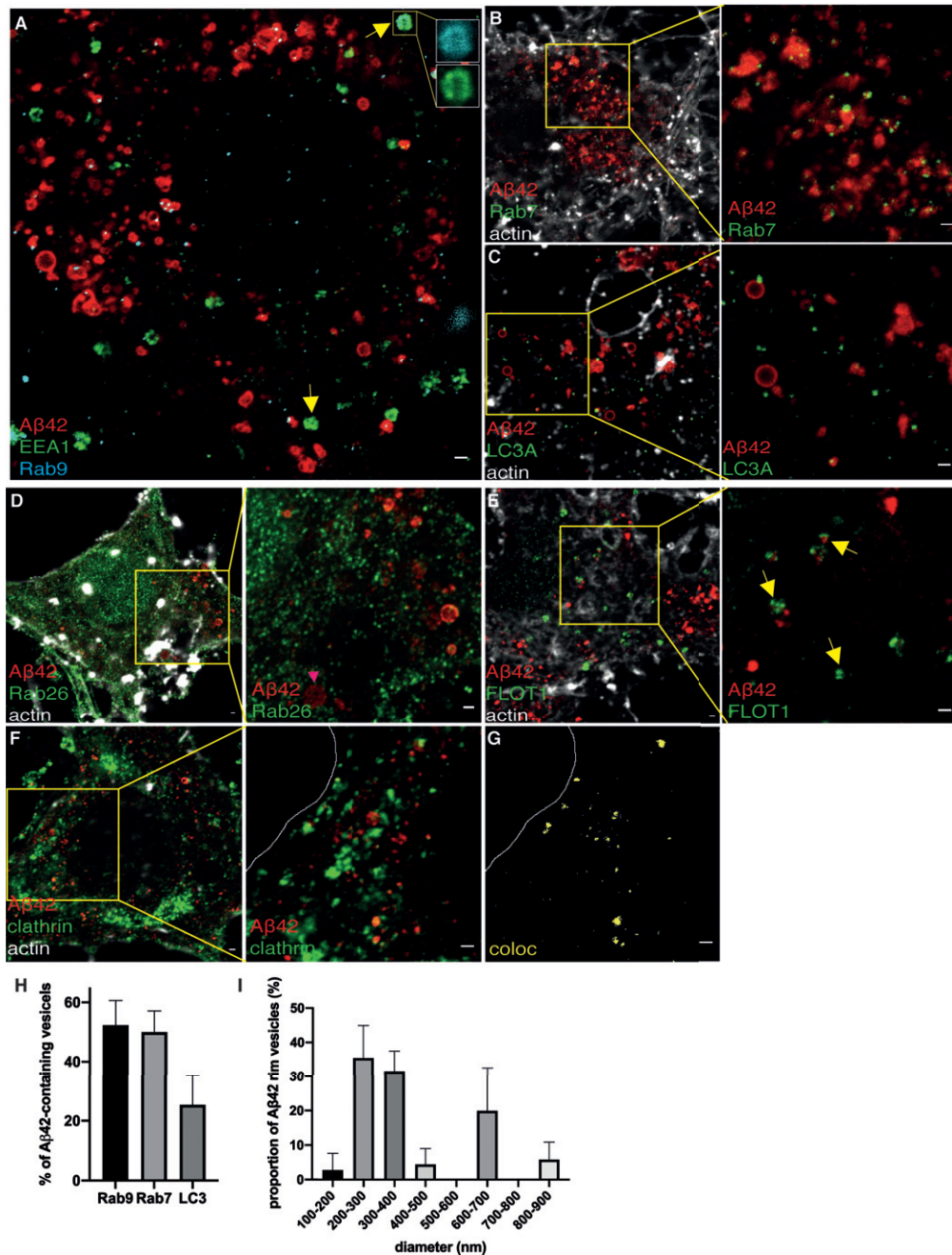
Fig. 5. STED images of Aβ$_{42}$ and subcellular markers in soma. A) 3-color STED image of Aβ42 (red), EEA1 (green), and Rab9 (cyan). (B-G) 2-channel STED imaging combined with actin staining (white) in a confocal channel. The zoomed-in pictures are shown to the right. B) Aβ$_{42}$ (red) and Rab7 (green). C) Aβ$_{42}$ (red) and LC3A (green). D) Aβ$_{42}$ (red) and Rab26 (green). E) Aβ$_{42}$ (red) and flotillin-1 (FLOT1, green). Yellow arrows point at areas rich in flotillin-1 containing vesicles. F) Aβ$_{42}$ (red) and clathrin (green). The white line marks the edge of soma. G) Colocalization between Aβ$_{42}$ and clathrin is shown in yellow. Scale bars for all pictures: 500 nm. H) Quantification of Aβ$_{42}$-containing vesicles in soma ($n = 20$ for each subcellular marker). Data were quantified from 3 different preparations of hippocampal neurons for each subcellular marker. All error bars represent mean ± sd. Analysis was done by "particle analyze" in ImageJ. Threshold "Moments" was applied for the Aβ$_{42}$ channel. Threshold "Triangle" was applied for subcellular markers channel. I) Quantification of the size (diameter) of vesicles containing Aβ$_{42}$ at the rim in soma. Data were quantified from 3 different batches of hippocampal neurons. Vesicles containing Aβ$_{42}$ at the rim were selected manually and 41 vesicles were quantified in total.
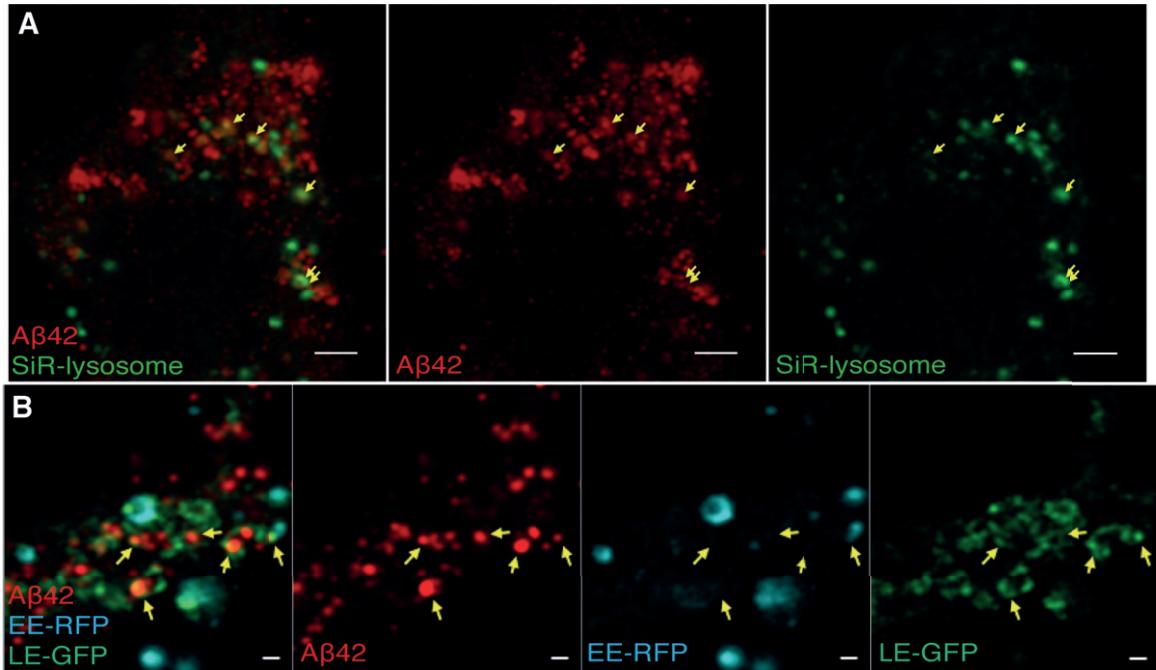
Fig. 6. Airyscan images of Aβ$_{42}$ and live cell labeled endosomes/lysosomes in soma. Cells were treated with live endosomal/cell markers, fixed, immuno-stained for Aβ$_{42}$ and imaged by confocal microscopy with an Airyscan detector. A) Aβ$_{42}$ (red) and SiR-lysosome (green). Scale bars: 2 μm. B) Aβ$_{42}$ (red), late endosome-GFP (LE-GFP) (green), early endosome-RFP (EE-RFP) (cyan). Colocalization is marked by yellow arrows. Scale bars: 500 nm.

have similar size as those that overlapped with Rab9. In synapses, no colocalization of Aβ$_{42}$ was observed with Rab9 or Rab7. The distribution of Rab26 was abundant in vesicles in dendrites and axons (Fig. 7F), and the vesicles had similar size as Rab26-containing vesicles in the soma. Some colocalization of Rab26 with Aβ$_{42}$ was observed in neurites, but not in synapses. FLOT1 did not show colocalization with Aβ42 in neurites (Supplementary Figure 5D). As in our previous study, high colocalization could be observed between Aβ$_{42}$ and synaptic vesicle markers in the presynaptic side in synapses, in this case Rab3 (Supplementary Figure 5E).

Overall, Aβ$_{42}$ vesicles showed different morphology in soma as compared to neurites, for instance the large vesicles containing Aβ$_{42}$ at the rim were rare in neurites compared to soma. Accumulation of small Aβ$_{42}$ vesicles was frequently observed in the presynapse, where they colocalized with clathrin and synaptic vesicle markers but not with endosomes or lysosomes. In contrast, the Aβ$_{42}$-containing vesicles in soma were larger and were positive for late endosomal, lysosomal and autophagosomal markers.

The subcellular locations of endocytosed, extracellular and endogenous Aβ$_{42}$ differ

To investigate the differences in trafficking of endogenous Aβ$_{42}$ versus Aβ$_{42}$ taken up from the medium, we added fluorescently labelled Aβ$_{42}$ to the medium of the neuronal cultures. Interestingly, exogenously derived Aβ$_{42}$ taken up by the neurons showed little or no colocalization with VAMP2 in presynapses, although it was present in neurites (Supplementary Figure 6), suggesting that the transport routes and final destination for Aβ$_{42}$ in the neurons differ depending on whether it is derived directly from endogenous synthesis in the same neuron or exogenously derived.

DISCUSSION

Super-resolution microscopy enables tremendously detailed studies of cellular processes [36]. This opens novel possibilities for research on neurodegenerative disorders such as AD, which is accompanied by synaptic degeneration and defects in vesicular transport. By using STORM and STED
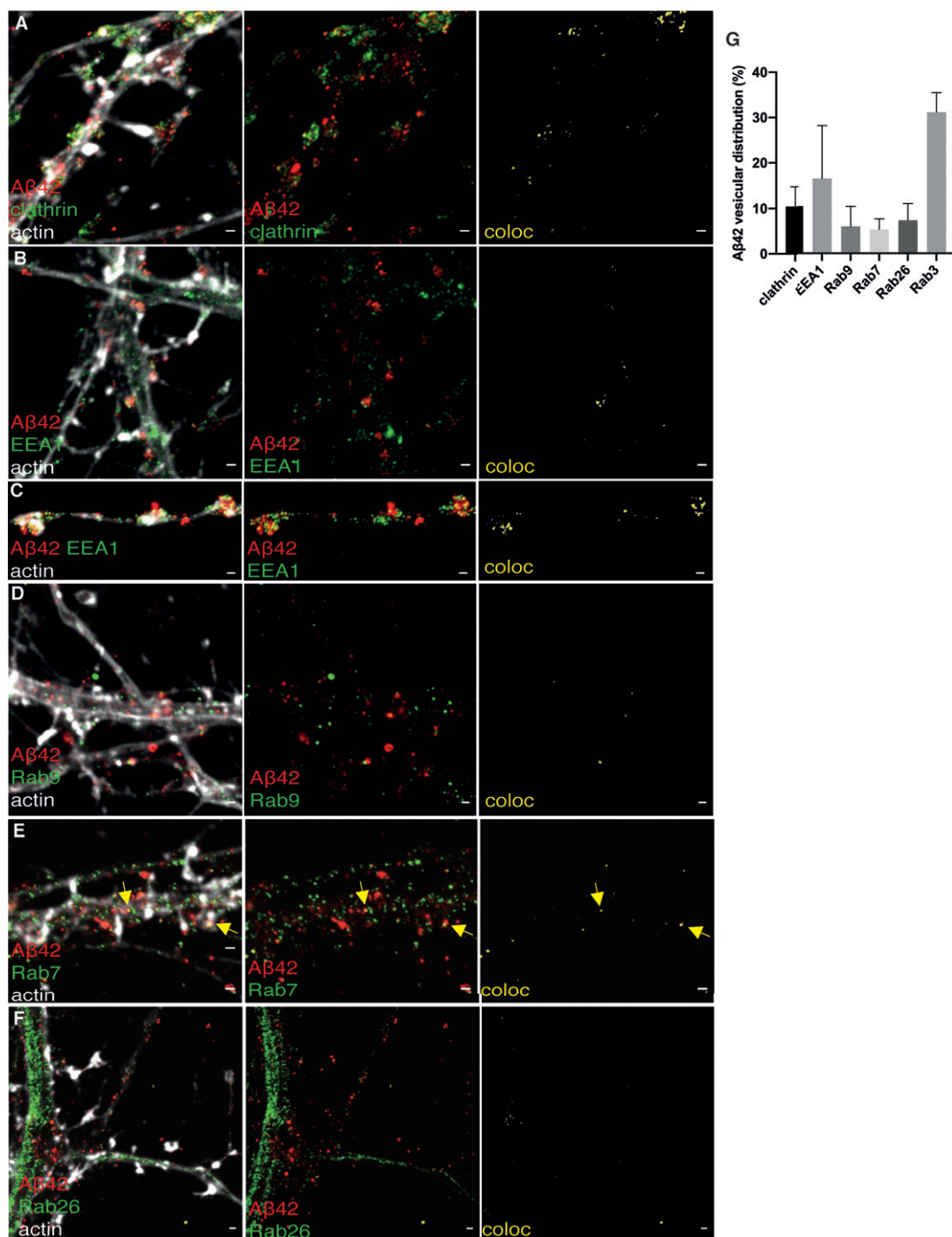
Fig. 7. STED images of $A\beta_{42}$ and subcellular markers in neurites. 2-channel STED imaging combined with actin staining (white) in a confocal channel. The colocalization between $A\beta_{42}$ and subcellular markers is shown to the right in yellow. A) $A\beta_{42}$ (red) and clathrin (green). B, C) $A\beta_{42}$ (red) and EEA1 (green). D) Staining of $A\beta_{42}$ (red) and Rab9 (green). E) $A\beta_{42}$ (red) and Rab7 (green). F) $A\beta_{42}$ (red) and Rab26 (green). Scale bars for all pictures: 500 nm. G) Distribution of Aβ42 staining in neurites. Data were quantified from 3 different batches of hippocampal neurons for each subcellular marker. All error bars represent mean ± sd. Analysis was done by "particle analyze" in ImageJ. Threshold "Moments" was applied for the $A\beta_{42}$ channel. Threshold "Triangle" was applied for the subcellular markers channel.
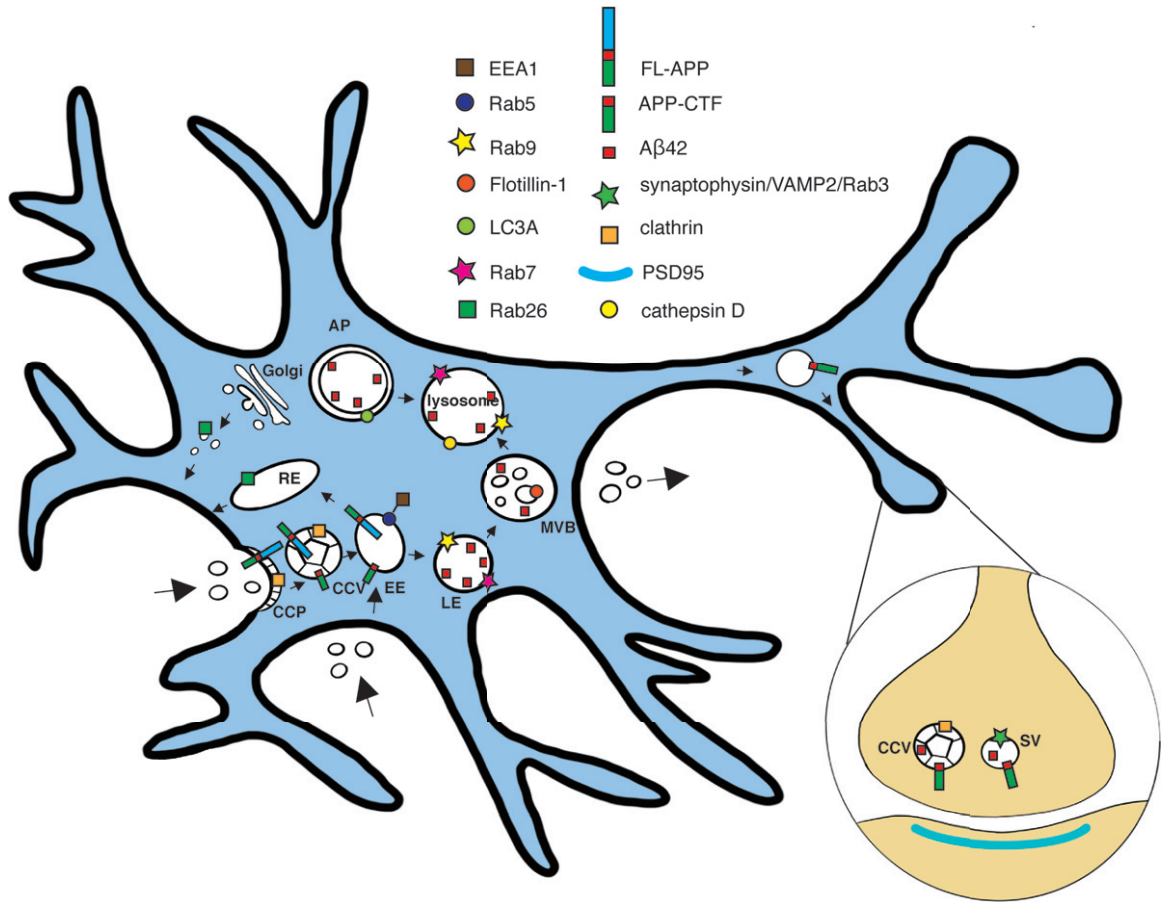
Fig. 8. Scheme of subcellular localization of full-length AβPP, CTFs, and/or Aβ$_{42}$ in hippocampal neurons. The subcellular localization of full-length AβPP (FL-APP), APP-C-terminal fragments (APP-CTF), and Aβ$_{42}$ in the endocytic-lysosomal system, based on STED imaging of hippocampal neurons, is shown. Early endosome antigen 1 (EEA1); clathrin coated vesicle (CCV); Early endosome (EE); Multi-vesicular body (MVB); Late endosome (LE); Autophagosome (AP); Synaptic vesicle (SV).

microscopy, we recently showed that γ-secretase is present both at the post- and presynaptic sides of synapses, while Aβ$_{42}$ is only present on the presynaptic side [28, 29]. In addition, we could resolve different types of Aβ$_{42}$-containing vesicles; small vesicles in the presynapse that partially colocalized with the synaptic vesicle protein synaptophysin and larger vesicles in other parts of the neurons that contain Aβ$_{42}$ only at the rim, i.e., at the luminal side of the membrane [29]. Based on those findings, we hypothesized that there are different pools of Aβ$_{42}$ that have different biological effects. These pools could differ in trafficking routes and subcellular localization. Further characterization of the nature, formation and localization of these pools along the neurons is thus critical for improved understanding of the mechanisms behind AD. Our data together with previous reports [37] suggest that the endosomal/lysosomal pathway is of high relevance for proteins involved

in AD. Hence, we have investigated the presence of Aβ$_{42}$ and its substrate AβPP along the endosomal-lysosomal pathways by using STED microscopy. The involvement of endocytosis in amyloidogenic AβPP processing has been studied for several years and it has for instance been shown that purified CCVs contain AβPP [38]. Our data from STED microscopy support the presence of APP-CT in CCPs and CCVs in hippocampal neurons. Interestingly, the ratio of CCPs to CCVs was higher in soma than in neurites. This finding may be related to a higher turnover rate in presynapses, since clathrin-mediated endocytosis is tightly connected to the synaptic vesicle cycle in presynapses, while it is important for recycling of receptors in soma/dendrites [35].

Considering that AβPP is taken up by clathrin-mediated endocytosis, it was not surprising that many (around 20%) of the APP-CT-containing particles in soma were present in early endosomes, which

arise after release of the clathrin-coat. In contrast to AβPP, endocytosis of BACE1 has been reported to be clathrin-independent [18, 19]. While several previous studies have suggested that BACE1 processing of AβPP occurs in early endosomes [39, 40], recycling endosomes have also been suggested as a site where BACE1 encounters AβPP [18]. To shed further light on this matter, we evaluated the presence of APP-CTF and APP-NTF in early endosomes. Due to the high resolution obtained by STED microscopy, and by including 3D 3-channel STED microscopy, it was possible to conclude that N- and C-terminal fragments were packed and sorted to different transport vesicles, seemingly budding out from early endosomes in different directions. Such sorting events are consistent with the observation that the different fragments are transported to different cellular localizations; NTF is secreted while APP-CTF is further processed into Aβ and AICD. In line with these findings, the retromer complex, known to be important for sorting events of early endosomes, has been shown to affect amyloidogenic processing of AβPP [41, 42].

The level of EEA1 decreases during development of early-early endosomes into late-early endosomes [43]. The positive correlation between the density of EEA1 in early endosomes and the level of APP-CT thus suggests that AβPP processing and sorting occurs early during early endosome maturation. This notion was supported by analyses of vesicles further downstream in the endo-lysosomal pathway, showing that APP-CT were absent or scarce in late endosomes.

Our data and several recent studies highlight the role of early endosomes in amyloidogenic AβPP processing. Enlargement of early endosomes have been reported in neurons in preclinical stages of AD [44]. Furthermore, genomic studies have led to identification of mutations in genes involved in early endosomal sorting that are associated to AD, including SORL1 [45] and components of the retromer complex, including VPS35 [46]. Human induced pluripotent stem cells (hIPSCs) carrying APP and/or PSEN1 FAD mutations have increased size of early endosomes [47]. Moreover, secretion of tau, another molecule involved in AD pathogenesis, was found to involve retromer-dependent endosomal recycling [48]. Altogether, these and our data support that defective endosomal trafficking plays a role in AD.

Overall, the colocalization between APP-CT and APP-NT was unexpectedly low, suggesting that a relatively low proportion of AβPP is the full-length form and that a large proportion of AβPP has been processed into CTFs and NTFs. The large pool of intracellular APP-CTF in vesicles may reflect a need for a substrate that rapidly can be processed by γ-secretase into Aβ, which besides its pathogenic role in AD has been suggested to have a physiological role for synaptic activity [16]. This notion is supported by the abundance of $A\beta_{42}$-containing vesicles overlapping with markers for synaptic vesicles and clathrin in the presynapse, as reported here and in our previous study [29]. Further support for synaptic involvement of $A\beta_{42}$ comes from our recent proteomic time-course study of $App^{NL/F}$ knock-in mice, which showed altered levels of several synaptic proteins months before the appearance of amyloid plaques and development of behavioral deficits [49].

The synaptic localization of AβPP has been a matter of debate. Our findings that APP-CTF but not full-length AβPP was present in the presynapse, while neither full-length AβPP nor APP-CTF was present at the postsynapse, is contradictory to some previous reports. This discrepancy could be explained by the limited resolution of conventional light microscopy used in many of the previous studies. In this context we would like to point out that we used STED microscopy, which enables a precision of around 20–30 nm in the x,y-plane. The STED microscope used here was calibrated to 43 nm resolution by using DNA origami nanorulers. Using 3D STED the calibrated resolution was around 100 nm along the z-axis, while around 500 nm along the z-axis using 2D STED. Thus, it is important to avoid overlap along the z-axis and consider the direction of the synapse. A previous study using super-resolution microscopy suggested that AβPP is present in both the pre- and postsynapse [50]. This may be due to some axons and dendrites being positioned on top of each other. Another study, using SIM microscopy and pre- and postsynaptic markers separated in the x-y plane (i.e. no overlap along the z-axis) showed presynaptic localization [51], in line with our findings. Here, we made sure to evaluate the synaptic localization only of synapses in images where the pre- and postsynaptic side were positioned side-by-side rather than on top of each other. Using this approach, we previously showed that γ-secretase and $A\beta_{42}$ are present in the presynapse [28, 29]. Hence, taken together with the current study, it is clear that the immediate substrate APP-CTF, γ-secretase and the product $A\beta_{42}$ itself, are all enriched at the presynapse, supporting the notion that $A\beta_{42}$ is formed at this compartment.

Early endosomes in the presynapse lack EEA1 [52]. Thus, the lack of colocalization of EEA1 with

APP-CTF or $A\beta_{42}$ does not exclude the possibility that early endosomes are present in the presynapse. One possible explanation for the absence of EEA1 in presynaptic early endosomes could be the need for a rapid vesicle cycle upon neuronal activity, where synaptic vesicles need to be formed rapidly and potentially may skip some steps such as coating of early endosomes with EEA1. Interestingly, $A\beta_{42}$ colocalized to a high extent with clathrin in some presynapses but to a low extent in others. This may be related to the fact that the majority of clathrin molecules are unassembled and concentrated outside of synaptic vesicle clusters under resting conditions and become scattered among de-clustered synaptic vesicles and move closer to the active zone upon depolarization [35]. Thus, the difference in distribution of $A\beta_{42}$ in relation to clathrin may reflect differences between various types of synapses, for instance depending on whether they are resting or active synapses, reflecting different mechanisms of endocytosis.

The synaptic vesicle cycle has been revisited during recent years [53]. Five mechanisms for vesicle endocytosis at the synapse have been suggested: clathrin-mediated endocytosis, bulk endocytosis, clathrin-independent fast endocytosis, ultrafast endocytosis and direct synaptic vesicle reformation through fast closure of a transient fusion pore (also referred to as kiss-and-run). As implied by the names, the contribution of clathrin differ between these mechanisms. Our data support that the generation of $A\beta$ from APP-CTF in the synapse occurs partly in connection to the clathrin-mediated synaptic vesicle cycle, since both APP-CTF and $A\beta_{42}$ colocalize with clathrin and synaptophysin, representing both the endocytic and synaptic vesicle components. In line with our findings, a recent article showed that conditional knock-out of presenilin in the pre-but not postsynapse in mice leads to impaired synaptic vesicle facilitation (a form of short-term plasticity that enhances synaptic transmission for less than a second) and reduced replenishment of release-competent synaptic vesicles [54].

In contrast to the presynapse, $A\beta_{42}$ was found at the rim of vesicles with sizes ranging from 100 to 900 nm in soma. The size distribution, with one peak at 200–300 nm and another peak at 600–700 nm, suggested that these were different organelles. In agreement with this finding, $A\beta_{42}$ colocalized with late endosomes, lysosomes and to some extent multivesicular bodies and autophagosomes. The lack of colocalization of APP-CTF and $A\beta_{42}$ in the same

vesicles in soma suggests that $A\beta_{42}$ is not formed to any great extent in this region. One possibility is that $A\beta_{42}$ in the soma derives from secreted $A\beta_{42}$ that has been taken up by endocytosis. The presence of $A\beta_{42}$ in somatic CCVs suggest that such uptake can occur via clathrin-mediated endocytosis in the soma.

Understanding the cell biology of $A\beta$ is necessary in order to elucidate the mechanisms behind, and find treatments against, AD. By using super-resolution microscopy, we have provided important insights about the distribution of components in the amyloidogenic pathway in neurons. Our study suggests that the first cleavage occurs in early endosomes, after clathrin-mediated endocytosis of AβPP. We further show that early endosomes in soma are important sorting organelles for AβPP fragments by budding and releasing transport vesicles containing NTFs or CTFs. The NTF vesicles can then be transported to the plasma membrane for secretion of NFTs while APP-CTFs are transported to the presynapse, where APP-CTF is cleaved. The cleavage appears to be associated with the synaptic vesicle cycle, since both APP-CTF and $A\beta_{42}$ colocalized with markers for synaptic vesicles and clathrin. These findings suggest that $A\beta_{42}$ present in the small vesicles in the presynapse is derived from synthesis in the same cell. In contrast, the large pool of $A\beta_{42}$ in soma appears to be derived from endocytosis of extracellular $A\beta_{42}$ [55]. The biological roles of those different pools of $A\beta_{42}$ are so far unclear. Although it is well-know that $A\beta$ is secreted, it has been debated whether such secretion occurs by an activity-dependent process. The secreted $A\beta_{42}$ probably acts by binding to postsynaptic receptors. However, it is also tempting to speculate that the $A\beta_{42}$ tightly packed in the presynapse may play a role in the synaptic vesicle cycle. We further propose that clathrin mediated endocytosis as well as synaptic $A\beta_{42}$ are relevant for both toxic and physiological functions of $A\beta_{42}$. Thus, elucidating their regulation is of utmost importance for precise targeting of $A\beta_{42}$ generation/oligomerization at neurotoxic intracellular localizations. Moreover, this study emphasizes the importance of using super-resolution microscopy to understand vesicular trafficking in neurons, which is of importance for many physiological and pathological conditions besides AD.

ACKNOWLEDGMENTS

Authors' disclosures available online (https://www.j-alz.com/manuscript-disclosures/21-5008).

SUPPLEMENTARY MATERIAL

The supplementary material is available in the electronic version of this article: https://dx.doi.org/10.3233/JAD-215008.

REFERENCES

[1] Söderberg L, Bogdanovic N, Axelsson B, Winblad B, Naslund J, Tjernberg LO (2006) Analysis of single Alzheimer solid plaque cores by laser capture microscopy and nanoelectrospray/tandem mass spectrometry. *Biochemistry* **45**, 9849-9856.

[2] Muller UC, Deller T, Korte M (2017) Not just amyloid: Physiological functions of the amyloid precursor protein family. *Nat Rev Neurosci* **18**, 281-298.

[3] Andrew RJ, Kellett KA, Thinakaran G, Hooper NM (2016) A Greek tragedy: The growing complexity of Alzheimer amyloid precursor protein proteolysis. *J Biol Chem* **291**, 19235-19244.

[4] Steiner H, Fluhrer R, Haass C (2008) Intramembrane proteolysis by gamma-secretase. *J Biol Chem* **283**, 29627-29631.

[5] Jan A, Hartley DM, Lashuel HA (2010) Preparation and characterization of toxic Abeta aggregates for structural and functional studies in Alzheimer's disease research. *Nat Protoc* **5**, 1186-1209.

[6] Hashimoto M, Bogdanovic N, Volkmann I, Aoki M, Winblad B, Tjernberg LO (2010) Analysis of microdissected human neurons by a sensitive ELISA reveals a correlation between elevated intracellular concentrations of Abeta42 and Alzheimer's disease neuropathology. *Acta Neuropathol* **119**, 543-554.

[7] Nilsson P, Loganathan K, Sekiguchi M, Matsuba Y, Hui K, Tsubuki S, Tanaka M, Iwata N, Saito T, Saido TC (2013)

Abeta secretion and plaque formation depend on autophagy. *Cell Rep* **5**, 61-69.

[8] Selkoe DJ, Hardy J (2016) The amyloid hypothesis of Alzheimer's disease at 25 years. *EMBO Mol Med* **8**, 595-608.

[9] Aoki M, Volkmann I, Tjernberg LO, Winblad B, Bogdanovic N (2008) Amyloid beta-peptide levels in laser capture microdissected cornu ammonis 1 pyramidal neurons of Alzheimer's brain. *Neuroreport* **19**, 1085-1089.

[10] Wilcox KC, Lacor PN, Pitt J, Klein WL (2011) Abeta oligomer-induced synapse degeneration in Alzheimer's disease. *Cell Mol Neurobiol* **31**, 939-948.

[11] De Strooper B, Karran E (2016) The cellular phase of Alzheimer's disease. *Cell* **164**, 603-615.

[12] Haass C, Selkoe DJ (2007) Soluble protein oligomers in neurodegeneration: Lessons from the Alzheimer's amyloid beta-peptide. *Nat Rev Mol Cell Biol* **8**, 101-112.

[13] Hallbeck M, Nath S, Marcusson J (2013) Neuron-to-neuron transmission of neurodegenerative pathology. *Neuroscientist* **19**, 560-566.

[14] Raskin J, Cummings J, Hardy J, Schuh K, Dean RA (2015) Neurobiology of Alzheimer's disease: Integrated molecular, physiological, anatomical, biomarker, and cognitive dimensions. *Curr Alzheimer Res* **12**, 712-722.

[15] Spires-Jones TL, Hyman BT (2014) The intersection of amyloid beta and tau at synapses in Alzheimer's disease. *Neuron* **82**, 756-771.

[16] Galanis C, Fellenz M, Becker D, Bold C, Lichtenthaler SF, Muller UC, Deller T, Vlachos A (2021) Amyloid-beta mediates homeostatic synaptic plasticity. *J Neurosci* **41**, 5157-5172.

[17] Guimas Almeida C, Sadat Mirfakhar F, Perdigao C, Burrinha T (2018) Impact of late-onset Alzheimer's genetic risk factors on beta-amyloid endocytic production. *Cell Mol Life Sci* **75**, 2577-2589.

[18] Das U, Scott DA, Ganguly A, Koo EH, Tang Y, Roy S (2013) Activity-induced convergence of APP and BACE-1 in acidic microdomains via an endocytosis-dependent pathway. *Neuron* **79**, 447-460.

[19] Sannerud R, Esselens C, Ejsmont P, Mattera R, Rochin L, Tharkeshwar AK, De Baets G, De Wever V, Habets R, Baert V, Vermeire W, Michiels C, Groot AJ, Wouters R, Dillen K, Vints K, Baatsen P, Munck S, Derua R, Waelkens E, Basi GS, Mercken M, Vooijs M, Bollen M, Schymkowitz J, Rousseau F, Bonifacino JS, Van Niel G, De Strooper B, Annaert W (2016) Restricted location of PSEN2/gamma-secretase determines substrate specificity and generates an intracellular Abeta pool. *Cell* **166**, 193-208.

[20] Edgar JR, Willen K, Gouras GK, Futter CE (2015) ESCRTs regulate amyloid precursor protein sorting in multivesicular bodies and intracellular amyloid-beta accumulation. *J Cell Sci* **128**, 2520-2528.

[21] Urbanelli L, Magini A, Buratta S, Brozzi A, Sagini K, Polchi A, Tancini B, Emiliani C (2013) Signaling pathways in exosomes biogenesis, secretion and fate. *Genes (Basel)* **4**, 152-170.

[22] Sardar Sinha M, Ansell-Schultz A, Civitelli L, Hildesjo C, Larsson M, Lannfelt L, Ingelsson M, Hallbeck M (2018) Alzheimer's disease pathology propagation by exosomes containing toxic amyloid-beta oligomers. *Acta Neuropathol* **136**, 41-56.

[23] Nilsson P, Sekiguchi M, Akagi T, Izumi S, Komori T, Hui K, Sorgjerd K, Tanaka M, Saito T, Iwata N, Saido TC (2015) Autophagy-related protein 7 deficiency in amyloid beta (Abeta) precursor protein transgenic mice decreases

Abeta in the multivesicular bodies and induces Abeta accumulation in the Golgi. *Am J Pathol* **185**, 305-313.

[24] Gouras GK, Tampellini D, Takahashi RH, Capetillo-Zarate E (2010) Intraneuronal beta-amyloid accumulation and synapse pathology in Alzheimer's disease. *Acta Neuropathol* **119**, 523-541.

[25] Brunholz S, Sisodia S, Lorenzo A, Deyts C, Kins S, Morfini G (2012) Axonal transport of APP and the spatial regulation of APP cleavage and function in neuronal cells. *Exp Brain Res* **217**, 353-364.

[26] Ross JA, Mathews PM, Van Bockstaele EJ (2019) High resolution approaches for the identification of amyloid fragments in brain. *J Neurosci Methods* **319**, 7-15.

[27] Takahashi RH, Milner TA, Li F, Nam EE, Edgar MA, Yamaguchi H, Beal MF, Xu H, Greengard P, Gouras GK (2002) Intraneuronal Alzheimer abeta42 accumulates in multivesicular bodies and is associated with synaptic pathology. *Am J Pathol* **161**, 1869-1879.

[28] Schedin-Weiss S, Caesar I, Winblad B, Blom H, Tjernberg LO (2016) Super-resolution microscopy reveals gamma-secretase at both sides of the neuronal synapse. *Acta Neuropathol Commun* **4**, 29.

[29] Yu Y, Jans DC, Winblad B, Tjernberg LO, Schedin-Weiss S (2018) Neuronal Abeta42 is enriched in small vesicles at the presynaptic side of synapses. *Life Sci Alliance* **1**, e201800028.

[30] Naslund J, Haroutunian V, Mohs R, Davis KL, Davies P, Greengard P, Buxbaum JD (2000) Correlation between elevated levels of amyloid beta-peptide in the brain and cognitive decline. *JAMA* **283**, 1571-1577.

[31] Martinsson I, Capetillo-Zarate E, Faideau M, Willen K, Esteras N, Frykman S, Tjernberg LO, Gouras GK (2019) APP depletion alters selective pre- and post-synaptic proteins. *Mol Cell Neurosci* **95**, 86-95.

[32] Fath T, Ke YD, Gunning P, Gotz J, Ittner LM (2009) Primary support cultures of hippocampal and substantia nigra neurons. *Nat Protoc* **4**, 78-85.

[33] Jones SA, Shim SH, He J, Zhuang X (2011) Fast, three-dimensional super-resolution imaging of live cells. *Nat Methods* **8**, 499-508.

[34] Bottanelli F, Schroeder L (2018) Stimulated emission depletion (STED) imaging of clathrin-mediated endocytosis in living cells. *Methods Mol Biol* **1847**, 189-195.

[35] Tao-Cheng JH (2020) Stimulation-induced differential redistributions of clathrin and clathrin-coated vesicles in axons compared to soma/dendrites. *Mol Brain* **13**, 141.

[36] Mockl L, Lamb DC, Brauchle C (2014) Super-resolved fluorescence microscopy: Nobel Prize in Chemistry 2014 for Eric Betzig, Stefan Hell, and William E. Moerner. *Angew Chem Int Ed Engl* **53**, 13972-13977.

[37] Whyte LS, Lau AA, Hemsley KM, Hopwood JJ, Sargeant TJ (2017) Endo-lysosomal and autophagic dysfunction: A driving factor in Alzheimer's disease? *J Neurochem* **140**, 703-717.

[38] Nordstedt C, Caporaso GL, Thyberg J, Gandy SE, Greengard P (1993) Identification of the Alzheimer beta/A4 amyloid precursor protein in clathrin-coated vesicles purified from PC12 cells. *J Biol Chem* **268**, 608-612.

[39] Rajendran L, Honsho M, Zahn TR, Keller P, Geiger KD, Verkade P, Simons K (2006) Alzheimer's disease beta-amyloid peptides are released in association with exosomes. *Proc Natl Acad Sci U S A* **103**, 11172-11177.

[40] Sannerud R, Declerck I, Peric A, Raemaekers T, Menendez G, Zhou L, Veerle B, Coen K, Munck S, De Strooper B, Schiavo G, Annaert W (2011) ADP ribosylation factor 6 (ARF6) controls amyloid precursor protein (APP) processing by mediating the endosomal sorting of BACE1. *Proc Natl Acad Sci U S A* **108**, E559-568.

[41] Bhalla A, Vetanovetz CP, Morel E, Chamoun Z, Di Paolo G, Small SA (2012) The location and trafficking routes of the neuronal retromer and its role in amyloid precursor protein transport. *Neurobiol Dis* **47**, 126-134.

[42] Small SA, Petsko GA (2015) Retromer in Alzheimer disease, Parkinson disease and other neurological disorders. *Nat Rev Neurosci* **16**, 126-132.

[43] Kamentseva R, Kosheverova V, Kharchenko M, Zlobina M, Salova A, Belyaeva T, Nikolsky N, Kornilova E (2020) Functional cycle of EEA1-positive early endosome: Direct evidence for pre-existing compartment of degradative pathway. *PLoS One* **15**, e0232532.

[44] Cataldo AM, Peterhoff CM, Troncoso JC, Gomez-Isla T, Hyman BT, Nixon RA (2000) Endocytic pathway abnormalities precede amyloid beta deposition in sporadic Alzheimer's disease and Down syndrome: Differential effects of APOE genotype and presenilin mutations. *Am J Pathol* **157**, 277-286.

[45] Thonberg H, Chiang HH, Lilius L, Forsell C, Lindstrom AK, Johansson C, Bjorkstrom J, Thordardottir S, Sleegers K, Van Broeckhoven C, Ronnback A, Graff C (2017) Identification and description of three families with familial Alzheimer disease that segregate variants in the SORL1 gene. *Acta Neuropathol Commun* **5**, 43.

[46] Rovelet-Lecrux A, Charbonnier C, Wallon D, Nicolas G, Seaman MN, Pottier C, Breusegem SY, Mathur PP, Jenardhanan P, Le Guennec K, Mukadam AS, Quenez O, Coutant S, Rousseau S, Richard AC, Boland A, Deleuze JF, Frebourg T, Hannequin D, Campion D, CNR-MAJ collaborators (2015) De novo deleterious genetic variations target a biological network centered on Abeta peptide in early-onset Alzheimer disease. *Mol Psychiatry* **20**, 1046-1056.

[47] Kwart D, Gregg A, Scheckel C, Murphy EA, Paquet D, Duffield M, Fak J, Olsen O, Darnell RB, Tessier-Lavigne M (2019) A large panel of isogenic APP and PSEN1 mutant human iPSC neurons reveals shared endosomal abnormalities mediated by APP beta-CTFs, not Abeta. *Neuron* **104**, 256-270 e255.

[48] Simoes S, Neufeld JL, Triana-Baltzer G, Moughadam S, Chen EI, Kothiya M, Qureshi YH, Patel V, Honig LS, Kolb H, Small SA (2020) Tau and other proteins found in Alzheimer's disease spinal fluid are linked to retromer-mediated endosomal traffic in mice and humans. *Sci Transl Med* **12**, eaba6334.

[49] Schedin-Weiss S, Nilsson P, Sandebring-Matton A, Axenhus M, Sekiguchi M, Saito T, Winblad B, Saido T, Tjernberg LO (2020) Proteomics time-course study of App knock-in mice reveals novel presymptomatic Abeta42-induced pathways to Alzheimer's disease pathology. *J Alzheimers Dis* **75**, 321-335.

[50] Kedia S, Ramakrishna P, Netrakanti PR, Jose M, Sibarita JB, Nadkarni S, Nair D (2020) Real-time nanoscale organization of amyloid precursor protein. *Nanoscale* **12**, 8200-8215.

[51] Rice HC, de Malmazet D, Schreurs A, Frere S, Van Molle I, Volkov AN, Creemers E, Vertkin I, Nys J, Ranaivoson FM, Comoletti D, Savas JN, Remaut H, Balschun D, Wierda KD, Slutsky I, Farrow K, De Strooper B, de Wit J (2019) Secreted amyloid-beta precursor protein functions as a GABABR1a ligand to modulate synaptic transmission. *Science* **363**, eaao4827.

[52]   Wilson JM, de Hoop M, Zorzi N, Toh BH, Dotti CG, Parton RG (2000) EEA1, a tethering protein of the early sorting endosome, shows a polarized distribution in hippocampal neurons, epithelial cells, and fibroblasts. *Mol Biol Cell* **11**, 2657-2671.

[53]   Chanaday NL, Cousin MA, Milosevic I, Watanabe S, Morgan JR (2019) The synaptic vesicle cycle revisited: New insights into the modes and mechanisms. *J Neurosci* **39**, 8209-8216.

[54]   Barthet G, Jorda-Siquier T, Rumi-Masante J, Bernadou F, Muller U, Mulle C (2018) Presenilin-mediated cleavage of APP regulates synaptotagmin-7 and presynaptic plasticity. *Nat Commun* **9**, 4780.

[55]   Gao Y, Wennmalm S, Winblad B, Schedin-Weiss S, Tjernberg LO (2021) Live cell FRET imaging reveals amyloid beta-peptide oligomerization in hippocampal neurons. *Int J Mol Sci* **22**, 4530.